Scientific Reports

https://doi.org/10.1038/s41598-026-54852-y

Article in Press

Ultra-sensitive label-free bio-detection via dielectric-modulated GOSC-SOI-TFET

Received: 27 February 2026

Accepted: 20 May 2026

Published online: 09 June 2026

Cite this article as: Kollapudi S.N.V. & Singh M.K. Ultra-sensitive label-free bio-detection via dielectric-modulated GOSC-SOI-TFET. *Sci Rep* (2026). https://doi.org/10.1038/s41598-026-54852-y

S. N. Vittal Kollapudi & Manish Kumar Singh

Ultra-Sensitive Label-Free Bio-Detection via Dielectric-Modulated GOSC-SOI-TFET

S. N. Vittal Kollapudi[1] **and Manish Kumar Singh**[1]

[1]School of Electronics Engineering, VIT-AP University, Inavolu, Guntur D.t.,522241, Andhra Pradesh, India.
[*]mksingh@vitap.ac.in

ABSTRACT

In this work, a highly sensitive label-free dielectric-modulated biosensor based on a Gate-Over-Source-Channel Silicon-on-Insulator Tunnel Field-Effect Transistor (GOSC-SOI-TFET) is proposed and systematically investigated. The novelty of the design lies in the asymmetric gate configuration with a strategically positioned nanocavity near the gate–source interface, providing enhanced electrostatic control and improved band-to-band tunneling (BTBT) efficiency. A comprehensive TCAD-based simulation framework, comprising non-local BTBT and trap-assisted tunneling models, is applied to assess the device reaction toward neutral and charged biomolecules. To achieve realistic operation, non-ideal factors like steric hindrance and non-uniform probe dispersion are also considered. The results demonstrate that the sensor sensitivity is substantially impacted by biomolecule location, with best performance achieved when analytes are situated near the source-channel tunneling junction. The proposed biosensor demonstrates an ON-current sensitivity of 6.09×10^8 for gelatin biomolecules, which is approximately $1.7\times$ higher than that of conventional TFET-based biosensors, while operating at a reduced drain voltage of $V_{ds} = 0.7$ V (about 30% lower). This highlights its potential for low-power and high-performance biomedical sensing applications.

Keywords: GOSC-SOI-TFET, Nanocavity, Label-free detection, Steric hindrance, Non-ideal hybridization, Biomedical sensing.

Introduction

Biosensors are essential components of modern analytical and diagnostic systems for rapid and selective detection of biological and chemical species. Traditional diagnostic methods, including laboratory-based biochemical tests, are usually time-consuming and require specialized equipment, which can lead to delayed results and, consequently, late diagnosis and treatment of diseases, especially in the case of chronic or rapidly progressing diseases[1]. On the other hand, biosensors enable real-time monitoring of biological and chemical signals, allowing early disease diagnosis, continuous health monitoring and personalized treatment strategies[2]. Biosensors are well suited for point-of-care diagnostics and management of chronic or age-related diseases due to their high sensitivity, portability, rapid response and ease of use[3]. Biosensors are classified into label-based and label-free in general[4–6]. Label-based detection approaches such as fluorescent, magnetic and electrochemical assays are based on the tagging of biomolecules by external markers. While these methods are useful in some applications, they can change the structural and functional properties of biomolecules, resulting in measurements that may not be accurate or reliable[7]. To overcome these limitations, label-free biosensors have attracted great attention owing to their simple design, low cost and the ability to detect biomolecules without modifying their intrinsic properties. Field-effect transistor (FET) based biosensors[8] have become a prominent technology in the class of label-free devices. These devices can transduce biochemical interactions into measurable electrical signals[9] with high sensitivity and selectivity, while preserving the integrity of biomolecules. Thus, FET-based biosensors have been utilized in disease diagnostics, drug development, environmental monitoring, and agricultural research[10]. The first ion-sensitive FET (IS-FET) biosensor[11] developed by Bergveld et al in 1970s could only detect charged biomolecules, which limited its scope of applications[12,13]. Various FET based architectures such as silicon nanowire FETs[14,15], FinFETs and silicon on insulator MOSFETs, have been widely investigated for biosensing applications. The FET-based biosensors have some notable advantages like small device size, low fabrication cost and high sensitivity[16]. However, they do have some inherent limitations. With the continuous scaling down of device geometries to the nanoscale, FET-based sensors face significant scaling challenges, such as short-channel effects (SCEs), drain-induced barrier lowering (DIBL), and subthreshold swing (SS) limitations governed by the kT/q factor[17,18]. All these effects degrade the device performance and lead to longer detection response times[19]. Tunnel FET (TFET)-based biosensors[20] have been proposed to address these limitations. Taking advantage of the band-to-band tunneling mechanism (BTBT) at the source-channel junction[21], TFETs exhibit a steep subthreshold swing (SS) (< 60 mV/decade)[22–24], lower leakage current, greater immunity to SCEs, and fast response times. Despite their advantages, However, TFETs have inherent limitations, such as low drive current and ambipolar conduction[25,26]. To address these problems, several structural modifications have been proposed, such as Dual-Gate (DG)[27,28], Gate-All-Around (GAA)[29,30], L-shaped[31],

and T-shaped[32,33] configurations which enhance electrostatic control and I_{ON}. At the same time, several TFET-based biosensor architectures have been investigated with nanocavities placed at different locations of the device, such as near the gate, drain, or source side[34–36] to facilitate dielectric modulation-based sensing. However, traditional TFET-based biosensors are still facing the challenges of low sensitivity and relatively high operating voltages, which hinder their applications in low-power, high-performance biosensing. In contrast, the proposed GOSC-SOI-TFET biosensor uses a double-gate structure, where the top gate is purposefully placed over the source and channel regions to get better electrostatic control and improved sensitivity. The device contains a nanocavity that is placed in a way that it affects both the gate and the source regions, thus enhancing the interaction of the biomolecule. Furthermore, the proposed structure has a simpler fabrication process and is compatible with the existing CMOS technology[37].

This is an outline of the current work's structure. The device architecture and simulation methodology are explained in Section 2. In order to assess practical applicability, Section 3 addresses the performance of the suggested design and looks at non-ideal phenomena such steric hindrance and uneven probe positioning. The suggested GOSC-SOI-TFET sensor is compared with earlier published research in Section 4. The investigation's key findings are finally presented in Section 5.

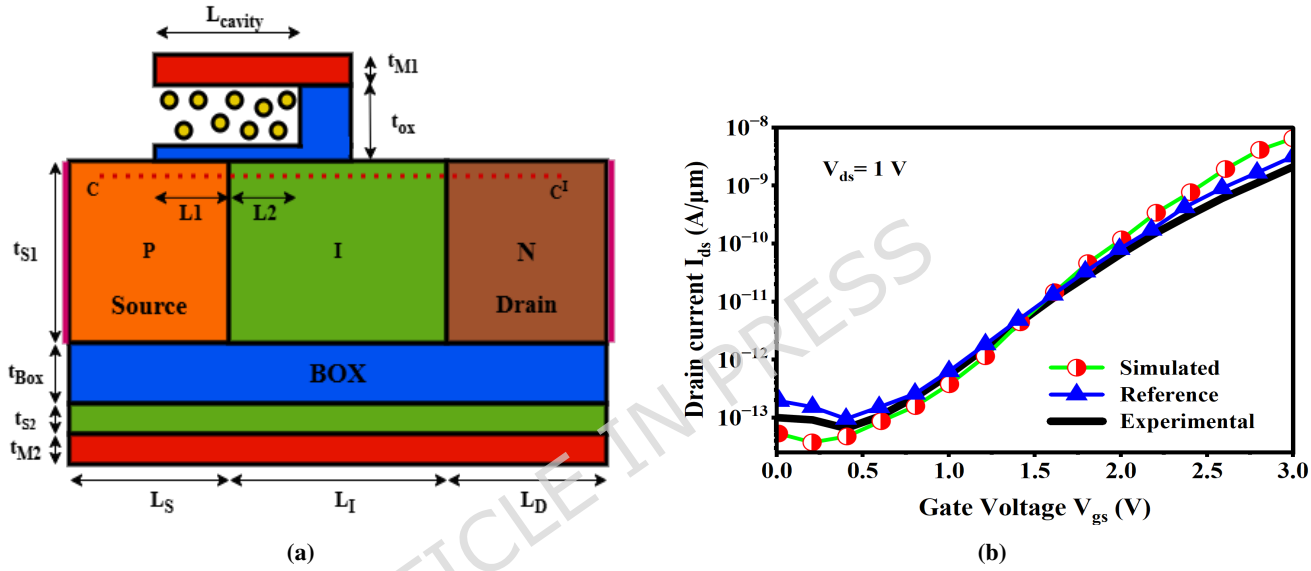

Fig. 1. (a) Proposed GOSC-SOI-TFET biosensor (b) Calibration of GOSC-SOI-TFET with experimental data[38] and reference work[39]

Architectures and simulation set-up

- Fabrication process flow

  Fig.2 illustrates the probable fabrication steps of the GOSC-SOI-TFET biosensor. Initially, the process begins with the deposition of a 10 nm thick buried oxide (BOX) layer on a moderately doped P-type silicon wafer ($1\times10^{16}\,cm^{-3}$) using a chemical vapor deposition (CVD) process. Next, the silicon layer is retained on top of the BOX, which serves as the source, channel, and drain regions. A thin film of SiO_2 was then deposited and uniformly coated with photoresist, after which the channel region was doped with arsenic impurities through an etching step. The intrinsic (I) channel region is then formed using ion implantation and rapid thermal annealing (RTA). Similarly, the process is followed to form the p^+ source region ($1\times10^{20}\,cm^{-3}$) and the n^+ drain region ($5\times10^{19}\,cm^{-3}$) as depicted in Table 1. Next, a 6 nm-thick oxide layer is grown using atomic layer deposition (ALD). Subsequently, metallization was performed using a sputter deposition process to form the electrical contacts. This was followed by selective etching of the metal and oxide layers, after which the surface was planarized using chemical mechanical polishing (CMP). Finally, selective etching of the oxide layer was carried out to define the bio-cavity region, and the exposed silicon area was passivated with a SiN protection layer, thereby completing the fabrication of the proposed GOSC-SOI-TFET biosensor. The resulting nanocavity serves as the active sensing region for biomolecule detection.

- Model details

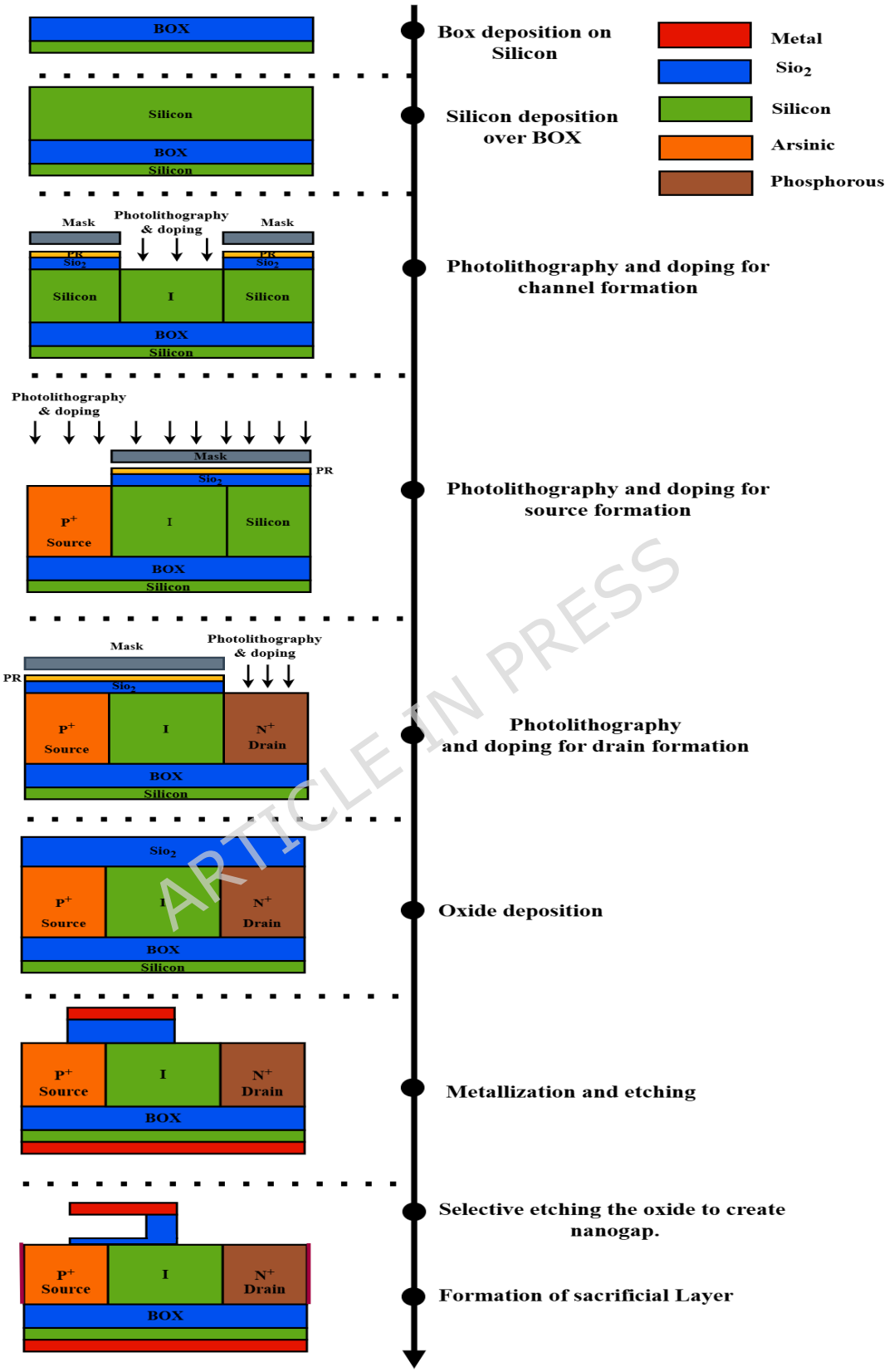

Fig. 2. Probable fabrication flow for GOSC-SOI-TFET biosensor

Table 1. Device parameters of GOSC SOI-TFET

Parameter	Value
Thickness of metal-1, t_{M1} (nm)	2
Bio-cavity thickness, t_{cavity} (nm)	5
Oxide thickness, t_{ox} (nm)	7
Bio-cavity length, L_{cavity} (nm)	20
Source length, L_S (nm)	30
Intrinsic region length, L_I (nm)	47
Drain length, L_D (nm)	30
Silicon-1 thickness, t_{S1} (nm)	30
Buried oxide thickness, t_{BOX} (nm)	10
Silicon-2 thickness, t_{S2} (nm)	5
Thickness of metal-2, t_{M2} (nm)	2
Gate metal work function (eV)	4.49
Source doping concentration (cm^{-3})	1×10^{20}
Intrinsic Si doping concentration (cm^{-3})	1×10^{16}
Drain doping concentration (cm^{-3})	5×10^{19}

All simulations in this work were performed using the Synopsys Sentaurus TCAD framework[40]. A non-uniform meshing scheme was adopted, with finer mesh in critical regions such as the tunneling junction, while a coarser mesh is used in other regions to optimize computational efficiency. Fermi–Dirac (FD) carrier statistics and Doping-Dependent Mobility (DDM) models are employed to obtain accurate carrier concentrations, electrostatic potentials, and mobility degradation under heavy doping conditions. The reduction in the semiconductor band gap arising from high doping and related physical effects is captured using an appropriate Band-Gap Narrowing (BGN) model. Carrier recombination through defect states within the forbidden gap is modeled using the SRH recombination mechanism. For a physically precise description of quantum-mechanical tunneling, the non-local BTBT model is employed, and the coefficients A and B are adjusted to fit the experimental results, taking values of $2.31\times10^{16}\,\text{cm}^{-1}\,\text{s}^{-1}\,\text{V}^{-2}$ and $3.58\times10^{6}\,\text{V}\,\text{cm}^{-1}$, respectively and Trap-Assisted Tunneling (TAT)[41] is also incorporated to account for defect-mediated tunneling pathways.

Results and discussion

In this section, the GOSC-SOI-TFET was analyzed using various biomolecules, including Uricase (a protein drug for infection suppression related to uric acid), APTES (for silanization purposes), Bacteriophage T7 (targets and kills various beneficial bacteria), keratin and gelatin (proteins present in nails, skin, and hair)[36], and MDA-MB231 and T47D (cancer cells). The dielectric constant (K) values of these biomolecules are provided in Table 2[42–45]. The analysis focused on evaluating the effects of both neutral and charged biomolecules (positively and negatively charged) within the sensor's cavity. By plotting their respective impacts, we gained insight into how these charges affect key device parameters. Finally, the influence of steric hindrance on hybridization and the deviation from ideal hybridization were investigated with respect to sensor sensitivity. Next, sensitivity (S) is a key parameter that describes the efficiency of a biosensor in detecting the biomolecules confined in a nanocavity. For reliable detection of target analytes, a high sensitivity value is desirable, as it directly reflects the biosensor's performance. Sensitivity is typically evaluated by comparing the device responses when the nanocavity is filled with biomolecules to those when it is vacant. The vacant nanocavity, which represents the absence of analytes, was treated as the reference condition (K = 1). Based on this approach, the sensitivity associated with the I_{ON} of the biosensor can be formulated[46] as given in (1)

$$S_{I_{\text{ON}}} = \frac{I_{ds}^{\text{Bio}}}{I_{ds}^{\text{Air}}} - 1 \tag{1}$$

In this expression, $S_{I_{ON}}$ represents the on-current sensitivity, I_{ds}^{Bio} denotes the I_{ON} measured in the presence of the target analyte, whereas I_{ds}^{Air} corresponds to the I_{ON} under the reference condition (air-filled cavity).

Selectivity is another key performance parameter of a biosensor that defines its ability to preferentially detect a specific target analyte in the presence of other potentially interfering species. It is evaluated based on the relative variation in drain current between two different biomolecules, as expressed in (2) selectivity, where ΔS denotes the selectivity between the target and non-target analytes:

$$\Delta S = \frac{I_{ds}^{\text{target}}}{I_{ds}^{\text{Non-target}}} - 1 \tag{2}$$

Table 2. Biomolecules and their K values.

Biomolecules	K- values
Uricase	1.54
APTES	3.57
Bacteriophage T7	6.3
Keratin	8.0
Gelatin	12.0
MDA-MB231	22.0
T47D	32.0

Impact of neutral charge biomolecules on sensitivity parameters

In this subsection, the impact of neutral biomolecules is analyzed by assuming that the nanocavity is filled (100% occupancy) with neutral biomolecules. The analysis was performed for various K values (1, 1.54, 3.57, 6.3, 8, 12, 22, and 32) at a drain voltage of 0.7 V and a gate voltage of 1.5 V. At this relatively low drain bias, the electric field near the drain region remains moderate, resulting in negligible hot carrier[47] generation and minimal reliability concerns. Furthermore, due to the band-to-band tunneling dominated transport in TFETs, the impact of hot carrier effects is significantly lower compared to conventional MOSFET devices, where $K = 1$ corresponds to a cavity filled with air. As the K of the biomaterial increases, the capacitive coupling between the gate and channel improves, leading to a reduction in the tunneling width, as illustrated in Fig. 3a. This narrowing of the tunneling width significantly enhanced the ON-state performance of the GOSC-SOI-TFET biosensor. Fig. 3b presents the transfer characteristics of the drain current (I_{ds}) as a function of gate voltage (V_{gs}) for different K values, revealing that higher K values produce greater I_{ON}, increasing from 2.94×10^{-15} to 1.04×10^{-4} A/μm. The corresponding energy-band diagram in the ON state is obtained by taking a horizontal cut-line located 1 nm beneath the oxide-silicon interface of the top gate[48], along with the electric field (E-field) distribution and the sensitivity comparison for the GOSC-SOI-TFET with neutral biomolecules at various K values, which are depicted in Fig. 3c and Fig.3d, respectively. The maximum $S_{I_{ON}}$ is reached 3.54×10^{10} when T47D biomolecules enter the cavity. To further assess the selectivity of the proposed biosensor, biomolecules such as keratin, bacteriophage T7, aptes and uricase are analyzed by comparing their corresponding drain current responses to the target biomolecule gelatin. The I_{ON} values for gelatin, keratin, bacteriophage T7, aptes, and uricase are 1.79×10^{-6}, 1.83×10^{-8}, 1.82×10^{-9}, 1.81×10^{-12} and 1.79×10^{-15} A/μm respectively. When the selectivity is assessed using (2), the results are 9.68×10^{1} for keratin, 9.83×10^{2} for bacteriophage T7, 9.89×10^{5} for aptes, and 2.25×10^{8} for uricase. These results show that, in comparison to the other biomolecules, gelatin achieves maximum selectivity to uricase.

Impact of positive charge biomolecules on sensitivity parameter

This subsection presents the simulation analysis of the GOSC-SOI-TFET biosensor incorporating positively charged biomolecules, with the K = 12 corresponding to Gelatin, and the nanocavity is assumed to be fully occupied (100% occupancy). The findings demonstrate that sensitivity increases with an increase in the magnitude of positively charged biomolecules from 1×10^{10} to 1×10^{12}. Fig. 4a and Fig.4e show the electrical and sensing characteristics of the GOSC-SOI-TFET in the presence of positively charged biomolecules. The electrostatic potential at the surface can be determined using the voltage balance equation of a metal-oxide-semiconductor[49], which describes how the charge density influences the sensitivity of the device.

$$V_{gs} = \Psi_s + \Phi_{ms} - \left(\frac{q(\pm N)}{C_{eff}}\right) \tag{3}$$

where Ψ_s, Φ_{ms}, q, C_{eff} represents the surface potential, work function difference between metal and semiconductor, unit charge, effective capacitance per unit area, and $N = N_{bio}$ represents the number of charged biomolecules per unit area[50]. Table 3 presents the equivalent capacitance networks and the corresponding effective capacitance formulas for the different nanogap profiles.

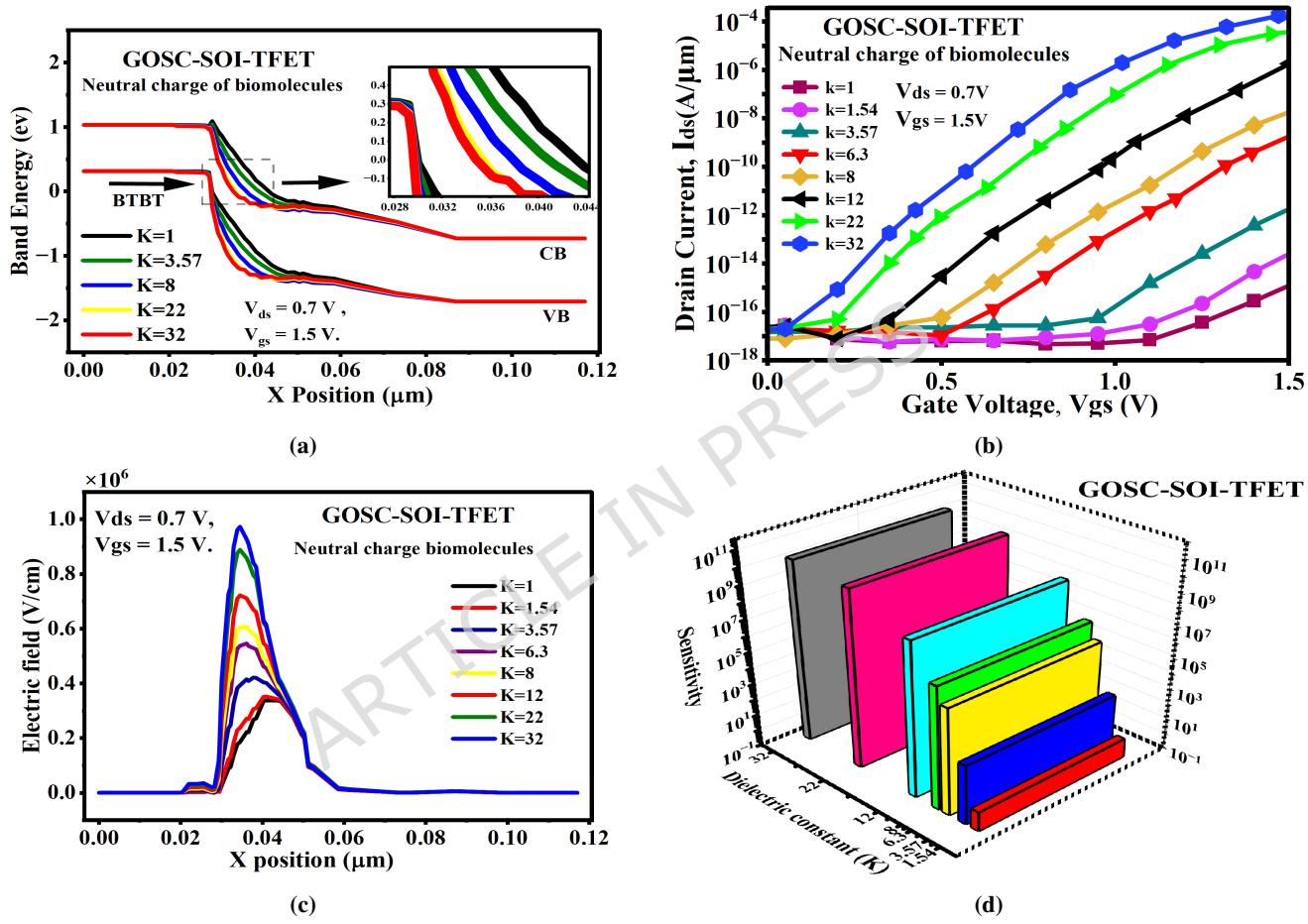

Fig. 3. (a) Energy-band profile in the ON state (b) Transfer characteristics (c) E-field distribution, and (d) Sensitivity comparison for the GOSC-SOI-TFET with neutral biomolecules at various K-values

$$\Psi_S = V_{gs} - \Phi_{ms} + \left(\frac{q(\pm N_{bio})}{C_{eff}}\right) \tag{4}$$

Table 3. Effective capacitance per unit area and equivalent circuit representations for different nanogap profiles.

Nanogap Profile	Illustration	Equivalent Capacitance Network	Effective Capacitance per Unit Area (C_{eff})
Fully filled profile (Uniform)[51]	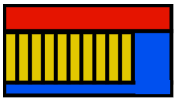	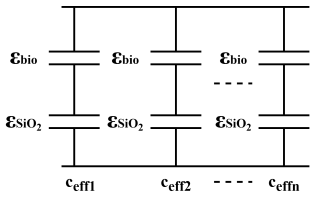	$\frac{\varepsilon_{\text{bio}}\,\varepsilon_{SiO_2}}{\varepsilon_{\text{bio}} t_{SiO_2} + \varepsilon_{SiO_2} t_{\text{bio}}}$
Presence and absence of biomolecule at the probe area		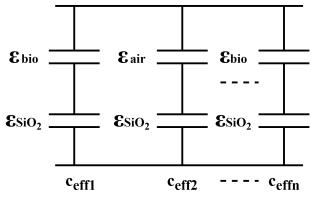	$C_{\text{eff,pres}} = \frac{\varepsilon_{\text{bio}}\,\varepsilon_{SiO_2}}{\varepsilon_{\text{bio}} t_{SiO_2} + \varepsilon_{SiO_2} t_{\text{bio}}}$ $C_{\text{eff,abs}} = \frac{\varepsilon_{\text{air}}\,\varepsilon_{SiO_2}}{\varepsilon_{\text{air}} t_{SiO_2} + \varepsilon_{SiO_2} t_{\text{air}}}$
Partially filled step profile (Non-Uniform)[52]	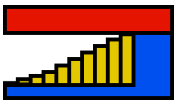	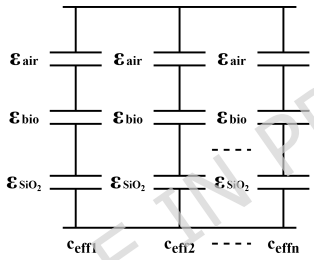	$\frac{\varepsilon_{\text{air}}\,\varepsilon_{\text{bio}}\,\varepsilon_{SiO_2}}{\varepsilon_{\text{bio}}\varepsilon_{\text{air}} t_{SiO_2} + \varepsilon_{SiO_2}\varepsilon_{\text{bio}} t_{\text{air}} + \varepsilon_{SiO_2}\varepsilon_{\text{air}} t_{\text{bio}}}$

As defined in (3), the concentration of positive charge ($+N_{bio}$) increases while keeping all other parameters (V_{gs}, q, C_{eff}) fixed, causes the term $\left(\frac{+qN_{bio}}{C_{eff}}\right)$ to increase, leading to an elevated surface potential Ψ_s. This rise in Ψ_s lowers the tunneling barrier height at the source-channel (S–C) interface. A reduced tunnel barrier improves the tunneling rate and therefore increases the I_{ON} from 1.83×10^{-6} to 3.39×10^{-6} A/μm as depicted in Table 4, which in turn improves the sensitivity. The same trend can be observed for the GOSC-SOI-TFET biosensors, as shown in Fig. 4b. which shows that $S_{I_{ON}}$ increases from 6.22×10^{8} to 1.15×10^{9}. Furthermore, there is a reduction in the V_t as illustrated in Fig. 4e, thereby reducing the required V_{gs}.

Impact of negative charge biomolecules on sensitivity parameter

Fig. 5a illustrates the energy band profile of the GOSC-SOI-TFET for various biomolecule charge densities ($N_{\text{bio}} = -1\times10^{10}$ to -1×10^{12} cm^{-2}), with a fixed $K = 12$ in the nanocavity. The findings show that the GOSC-SOI-TFET's energy band shifts in proportion to a decrease in N_{bio}. This phenomenon is explained by the E-field created by negatively charged biomolecules, which act against the device's current E-field. same has been From equ. (2), As the concentration of negative charges ($-N_{bio}$) increases while keeping all other parameters (V_{gs}, q, C_{eff}) fixed, the term $\left(\frac{-qN_{bio}}{C_{eff}}\right)$ decreases, resulting in a reduced Ψ_s. This decrease in Ψ_s results an elevated tunneling barrier at the S-C interface. An elevated tunnel barrier suppresses the tunneling rate, thereby reducing the I_{ON} from 1.82×10^{-6} to 9.42×10^{-7} A/μm and consequently lowering the device $S_{I_{ON}}$ from 6.17×10^{8} to 3.20×10^{8}. Furthermore, as shown in Fig. 5e, the V_t increases necessitate a higher V_{gs} for the device operation.

Effect of steric hindrance on hybridization within nanogaps

In the above analyses of the biosensor, it is generally assumed that the nanogaps are completely occupied with biomolecules, corresponding to an ideal fill factor (FF = 100%). Although this assumption simplifies the modeling process, it does not accurately reflect practical experimental conditions. In reality, when biomolecules enter the nanogap region, they interact with the receptors or probes and become immobilized on the cavity surface. This interaction leads to hybridization, in which biomolecules become bound to receptors. However, this hybridization process often halts before the cavity is fully occupied because the already immobilized biomolecules physically obstruct the entry of additional biomolecules into the remaining space.

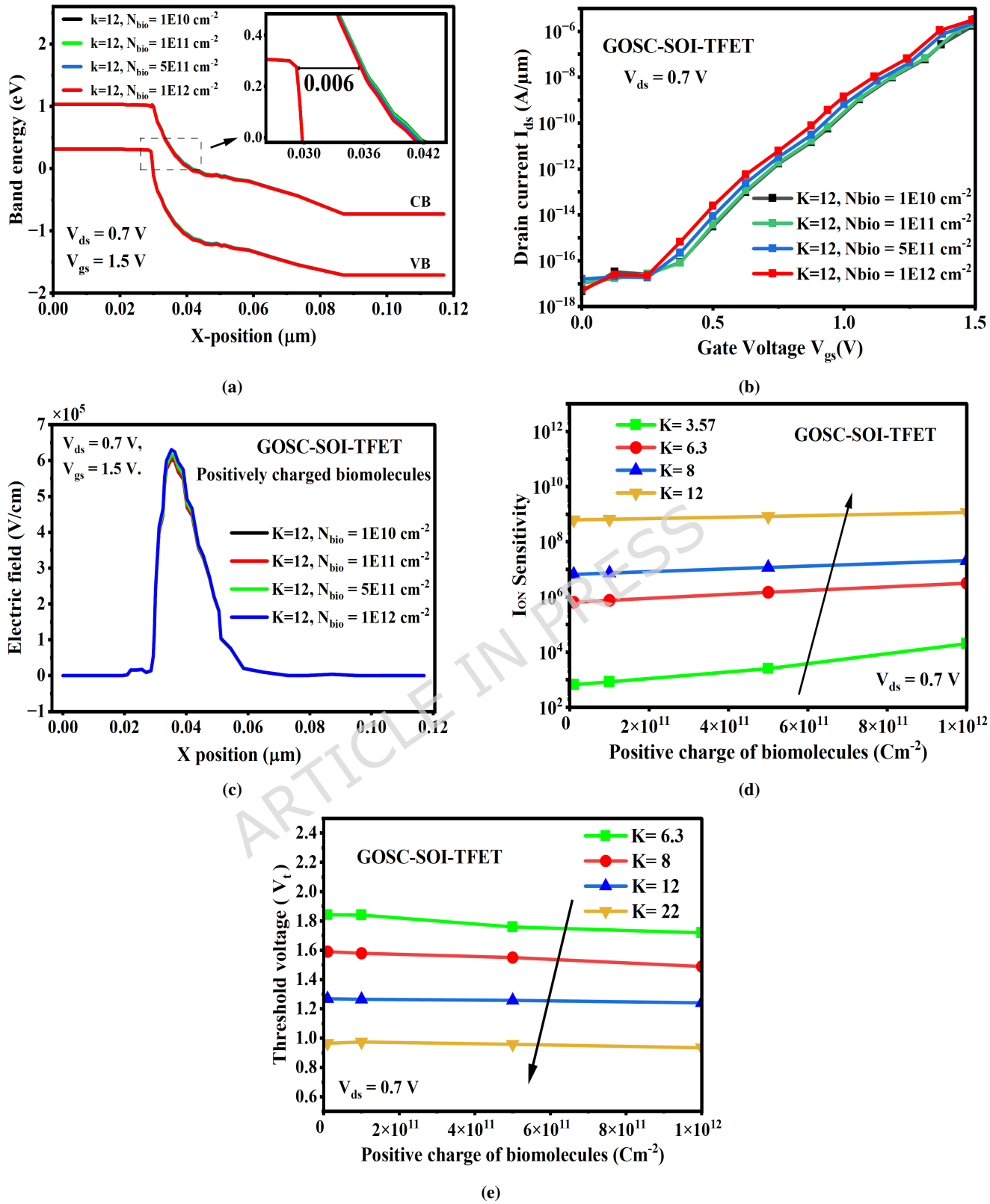

Fig. 4. GOSC-SOI-TFET with positively charged biomolecules: (a) Energy band-profile (b) Transfer characteristics (c) E-field distribution (d) Sensitivity with respect to the $+N_{bio}$, and (e) V_t shift as a function of $+N_{bio}$ for k = 6.3, 8, 12, and 22

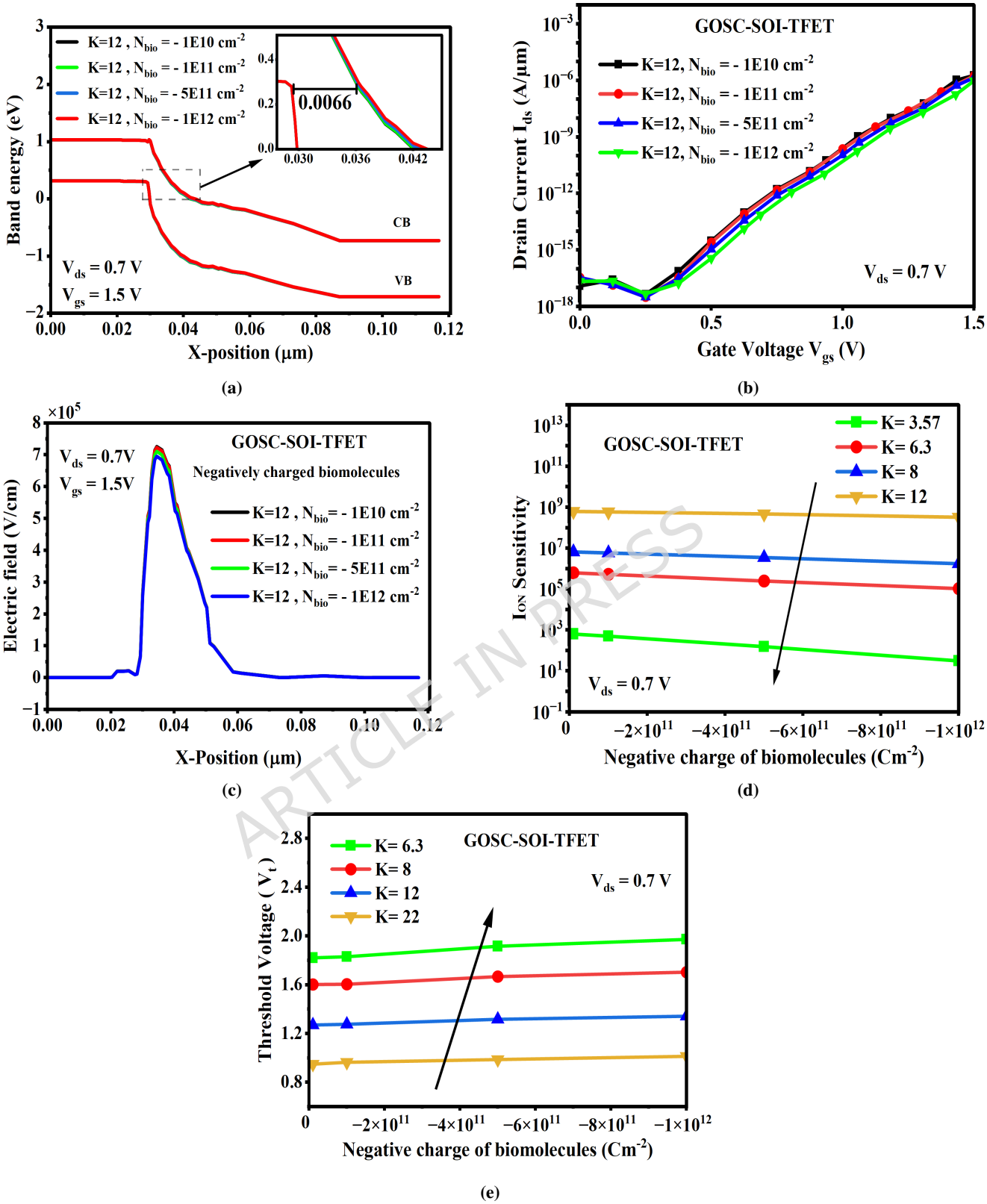

Fig. 5. GOSC-SOI-TFET with negatively charged biomolecules: (a) Energy band-profile (b) Transfer characteristics (c) E-field distribution (d) Sensitivity with respect to the $-N_{bio}$, and (e) V_t shift as a function of $-N_{bio}$ for k = 6.3, 8, 12, and 22

Table 4. GOSC-SOI-TFET sensitivity under varying dielectric properties and charge concentrations.

Applied Biomolecules	Dielectric Constant / Charge Density	$S_{I_{ON}}$ of GOSC-SOI-TFET
Neutral	$K = 1.54$	1.71×10^{0}
	$K = 3.57$	6.15×10^{2}
	$K = 6.3$	6.19×10^{5}
	$K = 8$	6.22×10^{6}
	$K = 12$	6.09×10^{8}
	$K = 22$	1.79×10^{10}
	$K = 32$	3.54×10^{10}
Positive	$K = 12,\ N_{bio} = 1 \times 10^{10}$	6.22×10^{8}
	$K = 12,\ N_{bio} = 1 \times 10^{11}$	6.56×10^{8}
	$K = 12,\ N_{bio} = 5 \times 10^{11}$	8.33×10^{8}
	$K = 12,\ N_{bio} = 1 \times 10^{12}$	1.15×10^{9}
Negative	$K = 12,\ N_{bio} = -1 \times 10^{10}$	6.17×10^{8}
	$K = 12,\ N_{bio} = -1 \times 10^{11}$	5.85×10^{8}
	$K = 12,\ N_{bio} = -5 \times 10^{11}$	4.63×10^{8}
	$K = 12,\ N_{bio} = -1 \times 10^{12}$	3.20×10^{8}

This phenomenon, known as steric hindrance, prevents the uniform occupation of nanogaps[53]. Due to steric hindrance, the spatial distribution of biomolecules within the cavity becomes highly non-uniform. Instead of forming a dense, homogeneous layer, the biomolecules are distributed in irregular patterns, which can manifest as increasing, decreasing, concave, or convex occupancy profiles along the nanogap region[54]. These non-uniform profiles reduce the effective FF to values below 100%, thus deviating from the ideal case used in the simulations. Such incomplete and asymmetric hybridization heavily affects the electrical response of the biosensor, ultimately reducing its sensitivity. Hence, while ideal fill-factor assumptions give an upper bound for performance, the actual behavior of nanogap TFET biosensors is strongly influenced by steric hindrance effects, which have to be taken into account for realistic modelling and design.[55].

The scenarios shown in Fig. 6 are examined, and the sensitivities are compared for four different nanocavity step profiles, all evaluated under a constant FF[56,57]. The length and thickness of the cavity region are 20 nm × 5 nm, resulting in a cavity area of 100 nm^2. This area is divided into ten segments, with each segment being maintained at a uniform length of 2 nm, ensuring a FF of 55% for the four considered conditions. A qualitative description of these configurations is summarized in Table 5. For the increasing step profile, the biomolecule density inside the nanogap is relatively low at the entrance and gradually increases toward the exit. The step heights increase progressively along the nanocavity with values of 0.5, 1.0, 1.5, 2.0, 2.5, 3.0, 3.5, 4.0, 4.5, and 5.0 nm, as shown in Fig. 6a. By reversing the beginning and end of the increasing step profile, a decreasing distribution is obtained, where the biomolecule density is highest at the entrance and gradually decreases toward the exit, as depicted in Fig. 6b. In the concave step profile, the step heights from the gap entry to the exit are 4.5, 3.2, 2.8, 2, 1.25, 1.25, 2, 2.8, 3.2, and 4.5 nm, as shown in Fig. 6c. This arrangement results in a concave distribution, with relatively higher biomolecule density at both ends of the nanogap and significantly lower biomolecule density at the center. The convex distribution profile is, on the other hand, the inverse of the concave step profile. In this configuration, the step heights start with increments from 1.25 to 4.5 nm and then decrease from 4.5 to 1.25 nm. As can be seen in Fig. 6d, here biomolecules are accumulated with higher density in the central region of the nanogap. The occupancy at both ends is relatively low.

A similar procedure is employed to maintain a FF of 80%. For each of the four cases, the step widths remain identical to those used in the earlier assessment, while the differences in step heights are approximately 0.5 nm for every two steps in both increasing and decreasing profiles. For the increasing step profile, the step heights are arranged as 3, 3, 3.5, 3.5, 4, 4, 4.5, 4.5, 5, and 5 nm. Reversing this sequence yields the decreasing profile. For the concave profile, the step heights are chosen as 5, 4.5, 4, 3.5, 3, 3, 3.5, 4, 4.5, and 5 nm. An opposite arrangement produces the convex step profile, where the step heights increase from 3 to 5 nm and then decrease from 5 to 3 nm. Fig. 7a and Fig. 7b illustrate how sensitivity varies with steric hindrance for fill factors of 55% and 80% at $N_{bio} = -5 \times 10^{11}$ cm^{-2}. From Fig. 7, $S_{I_{ON}}$ is consistently higher at the 80% fill factor, indicating that greater biomolecule occupancy within the nanocavity enhances electrostatic coupling and improves sensitivity. Among the four charge profiles examined, the increasing and concave distributions yield the highest $S_{I_{ON}}$ values due to their higher biomolecule concentration near the source side. In contrast, the decreasing profile exhibits the lowest sensitivity because the lower concentration near the tunneling region weakens its electrostatic influence, while the convex profile shows intermediate behavior. Overall, the observations confirm that steric hindrance effects play dominant roles in determining the biosensing performance of the GOSC-SOI-TFET.

Fig. 6. Possible irregular hybridization profiles arising from steric hindrance in the biosensors: (a) increasing (b) decreasing (c) concave and (d) convex profiles[58].

Table 5. Step profile alignment in nanocavity: biomolecule alignment model at fill factor = 55% and 80%.

Profile	FF = 55% (nm)	FF = 80% (nm)
Increasing	0.5, 1, 1.5, 2, 2.5, 3, 3.5, 4, 4.5, 5	3, 3, 3.5, 3.5, 4, 4, 4.5, 4.5, 5, 5
Decreasing	5, 4.5, 4, 3.5, 3, 2.5, 2, 1.5, 1, 0.5	5, 5, 4.5, 4.5, 4, 4, 3.5, 3.5, 3, 3
Concave	4.5, 3.2, 2.8, 2, 1.25, 1.25, 2, 2.8, 3.2, 4.5	5, 4.5, 4, 3.5, 3, 3, 3.5, 4, 4.5, 5
Convex	1.25, 2, 2.8, 3.2, 4.5, 4.5, 3.2, 2.8, 2, 1.25	3, 3.5, 4, 4.5, 5, 5, 4.5, 4, 3.5, 3

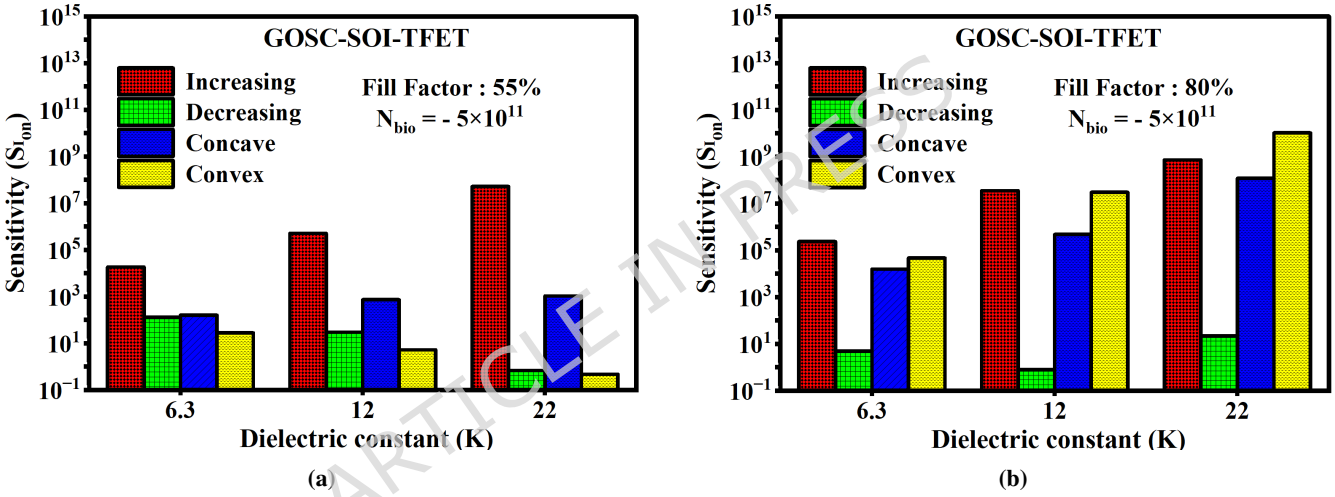

Fig. 7. Profiles of partially filled negative charge bio in nanogaps of GOSC-SOI-TFET with fill factor (a) 55 percent, (b) 80 percent

Effect of Non-Ideal Hybridization due to Probe/Receptor Positioning

In this section, the effect of non-ideal hybridization due to probe positioning is analyzed. The sensitivity of nanoscale biosensors is highly influenced by the spatial arrangement of the probes within the embedded nanogap. Because fully filling these nanogap is often challenging in practice, nonideal hybridization must be considered. The extent of hybridization between the probes and target biomolecules depends not only on the fraction of biomolecule-occupied regions but also on their precise locations within the cavity. Table 6 summarizes the different probe arrangements in the biosensors and their corresponding sensitivities for both positive positive ($N_{\text{bio}} = +5 \times 10^{11}\,\text{cm}^{-2}$) and negative ($N_{\text{bio}} = -5 \times 10^{11}\,\text{cm}^{-2}$) biomolecular charge densities. In table 6, the areas with asterisks (∗) indicates the existence of biomolecules ($k > 1$), whereas the blank areas represent air ($k = 1$). Sensitivity is generally maximized when biomolecules are located near the S–C interface. However, when biomolecules are positioned farther from the junction, the sensitivity decreases even if the overall biomolecule coverage within the nanogap remains the same. For instance, although case-5 & 6 both exhibit a FF of 60%, the $S_{I_{ON}}$ of the biosensor is higher in case-5. This is because a larger portion of the biomolecules in case-5 is located near the S–C interface, where the stronger E-field modulates the tunneling window more effectively, thereby enhancing sensitivity. These observations indicate that the biosensor performance is influenced not only by the total quantity of biomolecules present but also by their spatial distribution within the cavity.

Table 6. A comparison of threshold voltage and sensitivity at various probe locations inside the nanogap of GOSC-SOI-TFET biosensors for biomolecules carrying either positive or negative charges.

Case	Biomolecules										Total area occupied (%)	Positive charge of biomolecules				Negative charge of biomolecules			
	B_1	B_2	B_3	B_4	B_5	B_6	B_7	B_8	B_9	B_{10}		k=12		k=22		k=12		k=22	
												V_t	$S_{I_{ON}}$	V_t	$S_{I_{ON}}$	V_t	$S_{I_{ON}}$	V_t	$S_{I_{ON}}$
1								*	*	*	30	1.48	2.86×10^{6}	1.15	1.83×10^{8}	1.56	2.51×10^{7}	1.22	2.42×10^{9}
2						*	*	*			30	1.69	6.61×10^{6}	1.20	5.85×10^{9}	1.76	1.82×10^{6}	1.25	2.58×10^{9}
3		*		*		*		*		*	50	1.77	5.22×10^{5}	1.28	8.14×10^{7}	1.84	1.14×10^{6}	1.38	2.56×10^{8}
4	*		*		*		*		*		50	1.81	5.99×10^{5}	1.28	1.12×10^{9}	1.87	1.71×10^{5}	1.32	5.00×10^{8}
5					*	*	*	*	*	*	60	1.27	1.31×10^{8}	0.95	4.38×10^{9}	1.39	6.36×10^{8}	0.99	3.53×10^{10}
6		*		*		*		*	*	*	60	1.46	5.04×10^{6}	1.16	2.85×10^{8}	1.54	4.14×10^{7}	1.18	3.01×10^{9}
7	*		*	*		*	*	*		*	70	1.45	2.76×10^{7}	1.02	3.68×10^{8}	1.50	3.24×10^{7}	1.05	1.02×10^{10}
8		*	*	*	*		*		*	*	70	1.58	1.21×10^{6}	1.12	4.36×10^{8}	1.69	5.70×10^{6}	1.17	3.02×10^{9}
9	*		*	*	*	*	*		*	*	80	1.47	6.27×10^{6}	1.05	1.25×10^{9}	1.54	1.82×10^{7}	1.15	7.97×10^{9}
10	*	*	*		*	*		*	*	*	80	1.47	7.85×10^{6}	1.15	5.06×10^{8}	1.53	3.89×10^{7}	1.18	3.17×10^{9}

Table 7. Sensitivity comparison of the GOSC-SOI-TFET biosensor with other reported TFET biosensors while detecting the gelatin biomolecule.

Refs.	Biosensors	V_{ds}/V_{gs} (V)	Approximate Sensitivity $S_{I_{ON}}$
[59]	DM-DCTGTFET	1.0 / 2.0	1.4×10^{6}
[58]	N+ Pocket doped vertical TFET	1.0 / 1.5	1.56×10^{6}
[55]	HJ TFET	1.0 / 2.0	2.15×10^{6}
[60]	DC-DM HTFET	1.0 / 1.5	5×10^{6}
[56]	Hetero Stacked Source TFET	1.0 / 1.2	2.48×10^{7}
[57]	IT-CPTFET	1.0 / 1.5	1.18×10^{8}
[60]	SC-DM-EG HTFET	1.0 / 1.5	1.3×10^{8}
[55]	Circular Gate TFET	1.0 / 2.0	1.31×10^{8}
[56]	Heterostructure Vertical TFET	1.0 / 1.2	3.61×10^{8}
This work	**GOSC-SOI-TFET**	**0.7 / 1.5**	$\mathbf{6.09\times10^{8}}$

Comparison Report

The performance of the proposed GOSC-SOI-TFET biosensor is compared with some of the previously reported FET-based biosensing structures as listed in Table 7. Early devices such as DM-DCTGFET[59], N+ pocket doped vertical TFET[58] and HJ TFET[55] show moderate sensitivities at around 10^6. Improved designs, such as DC-DM HTFET[60] and HSS TFET[56], obtain better sensitivity values up to 2.48×10^7 due to higher electrostatic control and optimized cavity engineering. More advanced structures like IT-CPTFET[57], SC-DM-EG TFET[60], CG TFET[55], and HV TFET[56] push sensitivity into the 10^8 range, due to stronger dielectric modulation and better gate-channel coupling. On the other hand, the proposed GOSC-SOI-TFET exhibits a remarkably higher sensitivity of 6.09×10^8, which is greater than all the compared designs. This improvement is due to its gate-overlapped source configuration, effective charge modulation in the sensing cavity, and improved tunneling efficiency from the SOI platform.

Conclusion

A novel GOSC-SOI-TFET-based dielectric-modulated biosensor has been proposed and extensively analyzed for charged biomolecules. The incorporation of a dual-gate architecture along with a carefully engineered nanocavity enhances electrostatic control over the tunneling junction, resulting in improved band-to-band tunneling efficiency. Simulation results indicate that, for the gelatin biomolecule, the proposed device achieves the highest $S_{I_{ON}}$ compared to previously reported TFET-based biosensors. Charged biomolecules have a relatively minor impact on overall device performance, influencing sensitivity through surface potential modulation, where positive charges slightly enhance sensitivity with 1.15×10^9 while negative charges slightly suppress it to 3.20×10^8 by increasing the tunneling barrier height. Practical non-idealities, such as steric hindrance and non-ideal probe/receptor positioning, lead to non-uniform biomolecule distribution and reduced effective fill factors, thereby lowering sensitivity compared to ideal conditions. Despite these constraints, the device provides great sensitivity, exceeding conventional TFET biosensors at lower working voltage. These results demonstrate that the proposed biosensor is a promising candidate for the development of a cost-effective, low-power, and ultra-sensitive dielectrically modulated, label-free gelatin sensing application.

References

1. Dharmender, Nigam, K. K., Yadav, P. & Tikkiwal, V. A. Performance analysis of dual material control gate cavity on source electrically doped tfet biosensor for biomedical applications. *Micro Nanostructures* **191**, 207844, DOI: https://doi.org/10.1016/j.micrna.2024.207844 (2024).
2. Bind, M. K. & Nigam, K. K. Sensitivity and non-ideal issues analysis of a dielectric-modulated electrically doped junctionless tfet-based label-free biosensor. *IEEE Sensors J.* **24**, 24023–24030, DOI: https://doi.org/10.1109/JSEN.2024.3414311 (2024).
3. Wei, X. *et al.* Performance investigation of vertical tfet biosensor based on dual-source dual-channel trench gate. *Micro Nanostructures* **202**, 208129, DOI: https://doi.org/10.1016/j.micrna.2025.208129 (2025).
4. Raut, P., Panda, D. K. & Rashed, A. N. Z. Analysis of dual material gate insb/si heterojunction silicon on insulator tunnel field effect transistor (dmg-hj-soi-tfet) biosensor for creb-2 protein detection. *Sens. Imaging* **26**, 25, DOI: https://doi.org/10.1007/s11220-025-00558-w (2025).
5. Kumar, C. P. & Singh, M. K. Advanced biomolecule sensing: Simulation and sensitivity analysis of a dielectric-modulated bilayer electrode in dgotft. *Results Eng.* 107039, DOI: https://doi.org/10.1016/j.rineng.2025.107039 (2025).
6. Das, A., Rewari, S., Kanaujia, B. K., Deswal, S. & Gupta, R. Numerical modeling of a dielectric modulated surrounding-triple-gate germanium-source mosfet (dm-stggs-mosfet)-based biosensor. *J. Comput. Electron.* **22**, 742–759, DOI: https://doi.org/10.1007/s10825-023-02008-w (2023).
7. Singh, J., Wadhwa, G. & Raj, B. Design and sensitivity estimation of linear graded work function gate electrode hetero junction vertical tfet biosensor. *Microsyst. Technol.* **29**, 279–287, DOI: https://doi.org/10.1007/s00542-023-05424-x (2023).
8. Narang, R., Saxena, M. & Gupta, M. Comparative analysis of dielectric-modulated fet and tfet-based biosensor. *IEEE Transactions on Nanotechnol.* **14**, 427–435, DOI: https://doi.org/10.1109/TNANO.2015.2396899 (2015).
9. Harika, P., Kondavitee, G. S., Karumuri, S. R. & Lay-Ekuakille, A. High sensitivity of dielectrically modulated tunnel field effect transistor for biosensor applications. *IEEE Transactions on NanoBioscience* **24**, 25–36, DOI: https://doi.org/10.1109/TNB.2024.3386586 (2024).
10. Sravani Kondavitee, G., Anil Kumar, R. & Rao Karumuri, S. Design and performance analysis of n+ pocket-doped vertical dmdgdp tfet with t-shape channel for sensitivity improvement—as a biosensor. *IEEE Sensors J.* **25**, 3444–3451, DOI: https://doi.org/10.1109/JSEN.2024.3476693 (2025).

11. Singh, A. K., Tripathy, M. R., Baral, K. & Jit, S. Gasb/gaas type-ii heterojunction tfet on selbox substrate for dielectric modulated label-free biosensing application. *IEEE Transactions on Electron Devices* **69**, 5185–5192, DOI: https://doi.org/10.1109/TED.2022.3191295 (2022).

12. Bind, M. K., Singh, S. V. & Nigam, K. K. Design and performance evaluation of a heterojunction gaas/gasb pc-tfet for label-free biosensing applications: Mk bind et al. *J. Electron. Mater.* **54**, 1691–1708, DOI: https://doi.org/10.1007/s11664-024-11643-3 (2025).

13. Narang, R., Reddy, K. V. S., Saxena, M., Gupta, R. S. & Gupta, M. A dielectric-modulated tunnel-fet-based biosensor for label-free detection: Analytical modeling study and sensitivity analysis. *IEEE Transactions on Electron Devices* **59**, 2809–2817, DOI: https://doi.org/10.1109/TED.2012.2208115 (2012).

14. Das, A., Bhardwaj, A., Gupta, A. & Raj, G. Numerical comparative analysis of 10t-sram cells with 6t, 7t, 8t, and 9t using vertical nanowire tunnel fets. *Semiconductors* **59**, 427–435, DOI: https://doi.org/10.1134/S1063782625600299 (2025).

15. Yadav, S. & Rewari, S. Dual metal dual layer gaa nw–fet (dmdl–gaa–nw–fet) biosensor for label free sars-cov-2 detection. *Microsyst. Technol.* **30**, 565–582, DOI: https://doi.org/10.1007/s00542-023-05560-4 (2024).

16. Anand, S., Singh, A., Amin, S. I. & Thool, A. S. Design and performance analysis of dielectrically modulated doping-less tunnel fet-based label-free biosensor. *IEEE Sensors J.* **19**, 4369–4374, DOI: https://doi.org/10.1109/JSEN.2019.2900092 (2019).

17. Singh, D. *et al.* A charge-plasma-based dielectric-modulated junctionless tfet for biosensor label-free detection. *IEEE Transactions on Electron Devices* **64**, 271–278, DOI: https://doi.org/10.1109/TED.2016.2622403 (2016).

18. Harsha, N., Tiwari, S., Chaudhary, R. & Saha, R. Performances of gate stacked heterojunction selbox and soi tunnel fets including interface trap charges: A simulation study. *Mater. Sci. Eng. B* **300**, 117115, DOI: https://doi.org/10.1016/j.mseb.2023.117115 (2024).

19. Soni, D., Sharma, D., Aslam, M. & Yadav, S. Approach for the improvement of sensitivity and sensing speed of tfet-based biosensor by using plasma formation concept. *Micro & Nano Lett.* **13**, 1728–1733, DOI: https://doi.org/10.1049/mnl.2018.5252 (2018).

20. Singh, N. K., Kar, R. & Mandal, D. Simulation study of novel charge-plasma based arctfet for sensing the breast cancer biomarker (c-erbb-2) in serum. *IEEE Transactions on NanoBioscience* **22**, 554–561, DOI: https://doi.org/10.1109/TNB.2022.3216505 (2022).

21. Kanungo, S., Chattopadhyay, S., Gupta, P. S., Sinha, K. & Rahaman, H. Study and analysis of the effects of sige source and pocket-doped channel on sensing performance of dielectrically modulated tunnel fet-based biosensors. *IEEE Transactions on Electron Devices* **63**, 2589–2596, DOI: https://doi.org/10.1109/TED.2016.2556081 (2016).

22. Singh, J. & Singh, S. Improvement in the sensing performance of sige pocket si/ge vtfet based biosensor using extended source electrode and nano-cavity length. *Mater. Sci. Eng. B* **310**, 117688, DOI: https://doi.org/10.1016/j.mseb.2024.117688 (2024).

23. Kumar, C. P. & Singh, M. K. Ultra-high performance si0.5ge0.5 source hetero-dielectric tfet photosensor for near-infrared (nir) detection. *Micro Nanostructures* **208**, 208369, DOI: https://doi.org/10.1016/j.micrna.2025.208369 (2025).

24. Bhardwaj, A., Das, A., Sharma, U., Gupta, A. & Roy, S. Temperature induced analog performance modulation of high-k vertical nanowire tunnel fet. *Semiconductors* **59**, 382–390, DOI: https://doi.org/10.1134/S1063782625600020 (2025).

25. Tirkey, S., Sharma, D., Raad, B. R. & Yadav, D. S. A novel approach to improve the performance of charge plasma tunnel field-effect transistor. *IEEE Transactions on electron devices* **65**, 282–289, DOI: https://doi.org/10.1109/TED.2017.2766262 (2017).

26. Kumar, P., Koley, K. & Kumar, S. Comparative analysis of heavy ions and alpha particles impact on gate-all-around tfets and gate-all-around mosfets. *Micro Nanostructures* **192**, 207875, DOI: https://doi.org/10.1016/j.micrna.2024.207875 (2024).

27. Verma, M., Sharma, D., Pandey, S., Nigam, K. & Kondekar, P. Performance comparison of single and dual metal dielectrically modulated tfets for the application of label free biosensor. *Superlattices Microstruct.* **101**, 219–227, DOI: https://doi.org/10.1016/j.spmi.2016.11.045 (2017).

28. Dewan, B., Chaudhary, S. & Singh, D. Dc and rf/analog performances of dielectric-modulated split-source double gate tfet biosensor: A simulation study. *Mater. Sci. Eng. B* **313**, 117910, DOI: https://doi.org/10.1016/j.mseb.2024.117910 (2025).

29. Sakib, F. I., Hasan, M. A. & Hossain, M. Negative capacitance gate-all-around tunnel fets for highly sensitive label-free biosensors. *IEEE Transactions on Electron Devices* **69**, 311–317, DOI: https://doi.org/10.1109/TED.2021.3129711 (2022).

30. Kumar, P., Koley, K., Askari, S. S. A., Maurya, A. & Kumar, S. Assessment of negative bias temperature instability due to interface and oxide trapped charges in gate-all-around tfet devices. *IEEE Transactions on Nanotechnol.* **22**, 157–165, DOI: https://doi.org/10.1109/TNANO.2023.3255012 (2023).

31. Yang, Z. Tunnel field-effect transistor with an l-shaped gate. *IEEE electron device letters* **37**, 839–842, DOI: https://doi.org/10.1109/LED.2016.2574821 (2016).

32. Wang, Y. *et al.* Simulation study of dual metal-gate inverted t-shaped tfet for label-free biosensing. *IEEE Sensors J.* **22**, 18266–18272, DOI: https://doi.org/10.1109/JSEN.2022.3195180 (2022).

33. Bhardwaj, A., Das, A., Garg, P. & Yadav, S. Material-driven performance analysis of a vertical nanowire tunnel fet for analog applications: Bhardwaj, das, garg, and yadav. *J. Electron. Mater.* **55**, 1099–1110, DOI: https://doi.org/10.1007/s11664-025-12438-w (2026).

34. Das, A., Rewari, S., Kanaujia, B. K. & Gupta, R. Recent technological advancement in surrounding gate mosfet for biosensing applications-a synoptic study. *Silicon* **14**, 5133–5143, DOI: https://doi.org/10.1007/s12633-021-01288-w (2022).

35. Abdi, D. B. & Kumar, M. J. Dielectric modulated overlapping gate-on-drain tunnel-fet as a label-free biosensor. *Superlattices Microstruct.* **86**, 198–202, DOI: https://doi.org/10.1016/j.spmi.2015.07.052 (2015).

36. Patil, M., Gedam, A. & Mishra, G. P. Performance assessment of a cavity on source chargeplasmatfet-based biosensor. *IEEE Sensors J.* **21**, 2526–2532, DOI: https://doi.org/10.1109/JSEN.2020.3027031 (2020).

37. Fukata, N. Impurity doping in silicon nanowires. *Adv. Mater.* **21**, 2829–2832, DOI: https://doi.org/10.1002/adma.200900376 (2009).

38. Mayer, F. *et al.* Impact of soi, si 1-x ge x oi and geoi substrates on cmos compatible tunnel fet performance. In *2008 IEEE International Electron Devices Meeting*, 1–5, DOI: https://doi.org/10.1109/IEDM.2008.4796641 (IEEE, 2008).

39. Mitra, S. K. & Bhowmick, B. Impact of interface traps on performance of gate-on-source/channel soi tfet. *Microelectron. Reliab.* **94**, 1–12, DOI: https://doi.org/10.1016/j.microrel.2019.01.004 (2019).

40. Manual, S. D. U. Sentaurus device user manual. *CA, USA: Synopsys, Synopsys* (2022).

41. Elshafie, H. *et al.* Label-free biomolecule detection with inp/algaas charge plasma dielectric-modulated vertical tfet using tan as metal gate. *IEEE Access* DOI: https://doi.org/10.1109/ACCESS.2025.3570233 (2025).

42. Iqbal, M. Y., Alam, M. S., Anand, S. & Amin, S. I. A fom for investigation of sb tfet biosensor considering non-ideality. *IEEE Transactions on Nanotechnol.* **21**, 251–258, DOI: https://doi.org/10.1109/TNANO.2022.3178845 (2022).

43. Choudhary, V., Kumar, M., Chugh, N. & Madan, J. B-vdl-tfet: An ultrascaled, high-sensitivity sensor for breast cancer detection. *IEEE Sensors J.* **25**, 29820–29829, DOI: https://doi.org/10.1109/JSEN.2025.3581081 (2025).

44. Chowdhury, J., Mahapatra, K., Sarkar, A. & Das, J. K. An analytical model accounting for the pertinence of hybrid tunneling in bio-tfets. *IEEE Transactions on Nanotechnol.* **23**, 658–664, DOI: https://doi.org/10.1109/TNANO.2024.3462605 (2024).

45. Anil Kumar, R., Sravani Kondavitee, G., Wadhwa, G. & Rao Karumuri, S. A novel t-shape channel with an inverted-t nano-cavity label-free detection using si:hfo2 ferroelectric dgdm-jltfet as a biosensor—a simulation study. *IEEE Sensors J.* **24**, 37923–37931, DOI: https://doi.org/10.1109/JSEN.2024.3459100 (2024).

46. Kanungo, S., Chattopadhyay, S., Gupta, P. S. & Rahaman, H. Comparative performance analysis of the dielectrically modulated full-gate and short-gate tunnel fet-based biosensors. *IEEE Transactions on Electron Devices* **62**, 994–1001, DOI: https://doi.org/10.1109/TED.2015.2390774 (2015).

47. Kaul, A., Yadav, S., Rewari, S. & Nand, D. Computational modelling of cylindrical-ferroelectric-dual metal-nanowire field effect transistor (c-fe-dm-nw fet) using landau equation for gate leakage minimization. *Micro Nanostructures* **191**, 207851, DOI: https://doi.org/10.1016/j.micrna.2024.207851 (2024).

48. Kumar, M. J. & Janardhanan, S. Doping-less tunnel field effect transistor: Design and investigation. *IEEE transactions on Electron Devices* **60**, 3285–3290, DOI: https://doi.org/10.1109/TED.2013.2276888 (2013).

49. Tsividis, Y. & McAndrew, C. *Operation and Modeling of the MOS Transistor* (Oxford university press, 2011).

50. Liu, H. *et al.* Electron-hole bilayer tfet-based biosensor using hybrid tunneling mechanism for high off-state current and on-off current ratio sensitivities. *Micro Nanostructures* **207**, 208266, DOI: https://doi.org/10.1016/j.micrna.2025.208266 (2025).

51. Choi, J.-M., Han, J.-W., Choi, S.-J. & Choi, Y.-K. Analytical modeling of a nanogap-embedded fet for application as a biosensor. *IEEE transactions on electron devices* **57**, 3477–3484, DOI: https://doi.org/10.1109/TED.2010.2076152 (2010).

52. Devi, W. V., Bhowmick, B. & Pukhrambam, P. D. N+ pocket-doped vertical tfet for enhanced sensitivity in biosensing applications: modeling and simulation. *IEEE transactions on electron devices* **67**, 2133–2139, DOI: https://doi.org/10.1109/TED.2020.2981303 (2020).

53. Sen, D., Patel, S. D. & Sahay, S. Dielectric modulated nanotube tunnel field-effect transistor as a label free biosensor: proposal and investigation. *IEEE Transactions on NanoBioscience* **22**, 163–173, DOI: https://doi.org/10.1109/TNB.2022.3172553 (2022).

54. Das, D. & Pandey, C. K. A dielectrically modulated vertical tfet-based biosensor considering irregular probe placement and steric hindrance issues. *Micro Nanostructures* **190**, 207825, DOI: https://doi.org/10.1016/j.micrna.2024.207825 (2024).

55. Goswami, R. & Bhowmick, B. Comparative analyses of circular gate tfet and heterojunction tfet for dielectric-modulated label-free biosensing. *IEEE Sensors J.* **19**, 9600–9609, DOI: https://doi.org/10.1109/JSEN.2019.2928182 (2019).

56. Vanlalawmpuia, K. & Bhowmick, B. Analysis of hetero-stacked source tfet and heterostructure vertical tfet as dielectrically modulated label-free biosensors. *IEEE Sensors J.* **22**, 939–947, DOI: https://doi.org/10.1109/JSEN.2021.3128473 (2021).

57. Gorla, S. R. K. & Pandey, C. K. High-sensitivity detection in biosensors: A comparative study of inverted t-and l-channel charge plasma tfets. *Micro Nanostructures* **198**, 208060, DOI: https://doi.org/10.1016/j.micrna.2024.208060 (2025).

58. Wangkheirakpam, V. D., Bhowmick, B. & Pukhrambam, P. D. N+ pocket doped vertical tfet based dielectric-modulated biosensor considering non-ideal hybridization issue: A simulation study. *IEEE Transactions on Nanotechnol.* **19**, 156–162, DOI: https://doi.org/10.1109/TNANO.2020.2969206 (2020).

59. Kumar, S., Singh, Y., Singh, B. & Tiwari, P. K. Simulation study of dielectric modulated dual channel trench gate tfet-based biosensor. *IEEE Sensors J.* **20**, 12565–12573, DOI: https://doi.org/10.1109/JSEN.2020.3001300 (2020).

60. Mukhopadhyay, S., Sen, D., Goswami, B. & Sarkar, S. K. Performance evaluation of dielectrically modulated extended gate single cavity ingaas/si htfet based label-free biosensor considering non-ideal issues. *IEEE Sensors J.* **21**, 4739–4746, DOI: https://doi.org/10.1109/JSEN.2020.3033576 (2020).

Acknowledgements

The authors extend their sincere thanks to VIT-AP University and the C2S Program, funded by the Ministry of Electronics and Information Technology (MeitY), Government of India, for providing access to the Synopsis Sentaurus TCAD simulation software. This support was vital to the successful execution of the research, as the advanced features of the software enabled comprehensive analysis and contributed significantly to the study's outcomes. Additionally, Mr. S. N. Vittal Kollapudi conveys his gratitude to Prof. Chandan Kumar Pandey of the SENSE, VIT-AP University, for his assistance and expert perspectives which greatly enhanced the depth, quality, and direction of the work.

Author contributions

S. N. Vittal Kollapud: Design and analysis, writing original draft; **Manish Kumar Singh:** Review, editing, and supervision.

Additional information

Correspondence and requests for materials should be addressed to M.K.S.

Competing Interest:

The authors declare no competing interests.

Data and Material Availability:

The datasets used and/or analysed during the current study available from the corresponding author on reasonable request.